

Predicting sit-to-stand adaptations due to muscle strength deficits and assistance trajectories to complement them

Vinay Kumar^{1,*}, Takahide Yoshiike², and Tomohiro Shibata^{1,*}

¹Department of Human Intelligence Systems, Graduate School of Life Science and Systems Engineering, Kyushu Institute of Technology, Kitakyushu, Japan

²Honda R&D Co., Ltd., Saitama, Japan

Correspondence*:

Vinay Kumar
vinaym815@gmail.com

Tomohiro Shibata

tom@brain.kyutech.ac.jp

2 ABSTRACT

3

4 Sit-to-stand (STS) transition is one of the most bio-mechanically challenging task necessary
 5 for performing activities of daily life. With muscle strength being the most dominant, many co-
 6 occurring factors influence how individuals perform STS. This study investigates the changes in
 7 STS caused by muscle strength deficits and how they might lead to unsuccessful STS. It also
 8 presents the external assistance trajectories that can complement strength deficits for successful
 9 STS transition. Towards these aims, first, the single shooting optimization framework used to
 10 generate STS trajectories for musculoskeletal models with different strength deficits is presented.
 11 The muscle strength deficits were introduced by simultaneously scaling the maximum isometric
 12 strength of muscles in steps of 20%. The optimization framework could generate successful
 13 STS transition for models with up to 60% muscle strength deficits. Subsequently, for validation,
 14 the muscle activation patterns of the 0% strength deficit model are contrasted against those
 15 observed experimentally for a healthy subject. Then, the different strength deficit trajectories are
 16 compared to observe that when the vasti muscle gets saturated, the activation of the antagonistic
 17 hamstring muscle reduces to relieve it, leading to the saturation of the gluteus maximus muscle.
 18 Subsequently, this observation and the motion tracking results are used to suggest the vastus
 19 muscle weakness to be responsible for the breakdown of unassisted STS. Finally, the successful
 20 STS trajectory of the 80% strength deficit model when assisted externally at the torso is presented.
 21 The trajectory features utilization of external assistance as and when needed to complement
 22 strength deficits for successful STS transition. Our results will help plan intervention and design
 23 novel STS assistance devices.

24 **Keywords:** Sit-To-Stand, Musculoskeletal Model, Strength Deficit, Single Shooting Optimization, Open Loop Controller, Assist-A-
 25 Needed

1 INTRODUCTION

26 Sit-to-stand (STS) transition is a precursor to walking, hence critical for performing daily life activities
 27 and an independent lifestyle. Lower extremity strength plays an important role in human STS, and its
 28 deficits are thought to limit the STS functionality. Studies have shown that the lower extremity strength is a

29 strong predictor of the ability of older adults to perform STS from the lowest possible chair height (Hughes
30 et al., 1996; Schenkman et al., 1996). However, the decline in muscle strength often co-occurs with other
31 physiological and psychological impediments such as reduced balance, joint pain, and depression, making
32 it difficult to access its independent effect on STS using experiments (Lord et al., 2002). Also, besides
33 subject-specific factors, STS is influenced by many extrinsic factors like foot placement, knee position, and
34 chair height, making designing experiments complex.

35 Some past studies have used STS trajectories generated using optimization and musculoskeletal models
36 to avoid the complications of experiments (Pandy et al., 1995; Bobbert et al., 2016; Yokota et al., 2016).
37 Pandy et al. (1995) presented a cost function that generates STS trajectories with similar muscle activations
38 to those of experiments. Bobbert et al. (2016) and Yokota et al. (2016) searched for trajectories that reduced
39 loads on the muscles and the knee joint. However, the studies mentioned above have made either minimal
40 or no observations about STS changes caused by strength deficits. Further, these studies have also not
41 investigated how strength deficits might lead to unsuccessful STS.

42 Many older individuals incapable of independent STS transition can perform the same when aided
43 externally. This external assistance can help maintain or recover lower extremity strength when provided in
44 an assist-as-needed manner. Thus it is desirable to generate reference assistance trajectories that assist as
45 and when needed and by the amount needed for successful STS transition. Mombaur and Hoang (2017)
46 and Geravand et al. (2017) have used optimization to discover assistance trajectories that support part of the
47 user's weight during STS and squat-to-stand motions, respectively. However, both the studies use human
48 models with independently torque actuated joints. The hamstrings and the rectus femoris are two biarticular
49 muscles that play an essential role in the STS transition. Their biarticularity couples the torques produced
50 at the hip and knee joints. This coupling should not be ignored, especially when generating STS assistance
51 trajectories, as it may lead to over actuation of one of these muscles, leading to muscle contracture and
52 eventually lower back issues. The coupling is also crucial for the proper investigation of the STS changes
53 and the STS failure caused by the strength deficits.

54 This study aims to identify the changes in STS caused by muscle strength deficits, investigate how
55 they might lead to unsuccessful STS transition, and generate the external assistance trajectories that can
56 complement muscle strength deficits for successful STS transition. Towards these aims, we will first present
57 the single shooting optimization framework used to generate the STS trajectories for musculoskeletal
58 models with varying degrees of strength deficit. Then we contrast the joint angle trajectories, muscle
59 activation patterns, the ground and seat reaction forces from the STS trajectory of the 0% strength deficit
60 model against those of a healthy adult for validation. Subsequently, the different strength deficit trajectories
61 are compared to observe the changes in STS caused by strength deficits. Then, the motion-tracking results
62 are used to investigate the STS breakdown. Finally, the optimization framework's ability to generate
63 externally assisted STS trajectory is demonstrated for a musculoskeletal model incapable of performing
64 unaided STS transition. The findings of this study will help plan intervention and design novel STS
65 assistance devices that operate in an assist-as-needed manner.

66 Within the single shooting optimization framework, we have parameterized the open-loop excitation
67 trajectories of the actuators similarly to Pandy et al. (1995), and Yokota et al. (2016). The excitation
68 trajectories are used to integrate the system's equation motion of the equation forward in time. Then the
69 resultant motion is then used to tune the actuator's excitation trajectories. Another possible structure of
70 the optimization framework is one in which joint angle trajectories are parameterized. These frameworks
71 use the inverse dynamics solutions in the case of skeletal models (Yoshioka et al., 2007; Sadeghi et al.,
72 2013; Norman-Gerum and McPhee, 2018; Yang and Ozsoy, 2020) or the inverse dynamics plus static

73 optimization solutions in the case of musculoskeletal models (Yoshioka et al., 2012) to tune the joint angle
74 trajectories. Such a framework is used with a skeletal model in Yang and Ozsoy (2021), and Ozsoy and Yang
75 (2021) to predict the unilateral grab-rail assisted STS trajectories of a virtually unhealthy adult. Another
76 possible optimization framework is that of direct collocation in which the optimization is performed over
77 both the joint angle and the actuator excitation trajectories Bobbert et al. (2016). We selected open-loop
78 single shooting trajectory optimization for its straightforward implementation and effortless extension to
79 incorporate closed-loop controllers in future works.

80 It is not easy to identify and detail all of the parameters that shape the STS trajectories generated
81 using optimization. For example, Bobbert et al. (2016), and Yokota et al. (2016) does not contain
82 information about the initial guesses to the optimization algorithm, while Pandy et al. (1995) does
83 not include information about the mechanical limits used to restrict the motion to the physiologically
84 plausible range. Therefore we have made all the source code and results from this study public at
85 <https://github.com/ShibataLab/PredictiveSTS>.

2 METHODS

86 An overview of the single shooting optimization framework used to solve the dynamic optimization problem
87 of generating STS simulations in this study is shown in Figure 1. The optimization framework tunes the
88 values of decision variables using the aCMA-ES algorithm (Arnold and Hansen, 2010). aCMA-ES is a
89 stochastic gradient-free optimization algorithm that adapts a Gaussian distribution towards low energy
90 regions and was selected for its enhanced robustness to the locally optimal solution compared to the
91 gradient-based algorithms. At each generation, aCMA-ES samples a batch of candidate solutions from
92 the Gaussian distribution being adapted. Subsequently, the cost function values are computed for all the
93 candidates by running forward simulations. aCMA-ES then adapts the Gaussian distribution based on the
94 cost function values and proceeds to the next generation and so on until one of the stopping criteria is met.

95 In subsection 2.1, the musculoskeletal models used to generate STS trajectories with the optimization
96 framework are detailed. Subsection 2.2 includes the details of the decision variables and the termination
97 criteria used with the optimization framework, while subsection 2.3 describes the cost function. In
98 subsection 2.4 the motion-tracking setup used to investigate STS failure is summarized. The final subsection,
99 i.e., 2.5 lists the process steps for the experimental data used to validate the STS trajectory of the 0%
100 strength deficit model.

101 2.1 Musculoskeletal Model

102 Musculoskeletal models with different strength deficits for this study were obtained by simultaneously
103 scaling the maximum isometric strengths of the muscles present within the base model. The base model,
104 also shown in Figure 2, is a simplified version of the LaiArnold2017 model (Lai et al., 2017). The
105 LaiArnold2017 model represents an average-sized adult male of mass 75Kg and height 170cm. The base
106 model is two-dimensional with eight hill-type muscles and three degrees of freedom, while the source
107 model is 3D with 80 hill type muscles and 37 degrees of freedom. The simplifications were needed to
108 make the optimization problem computationally tractable. The following paragraph detail some of these
109 simplifications.

110 From the LaiArnold2017 model, the left leg and the associated muscle were removed. The masses of
111 arms, forearms, hands and the head were lumped to the torso's center of mass (COM). The mass and inertia
112 of the torso after lumping were halved to account for the missing left leg and associated muscles. The
113 right foot was fixed to the ground using a weld joint. Then the degrees of freedom corresponding to the

114 motion of the ankle, knee, hip and lumbar joints in the sagittal plane were added. The 0° angle of the
115 hip, knee, ankle and lumbar joints corresponds model standing upright. From 0° , the positive joint angles
116 correspond to ankle dorsiflexion, knee flexion, hip flexion, and lumbar extension; and negative joint angles
117 correspond to the opposite. The lumbar joint was locked to -10° , and thus the model effectively has three
118 degrees of freedom. The lower extremity muscles with similar functions from the LaiArnold2017 model
119 were combined to single muscle-tendon units as is realized in Ong et al. (2019). Figure 2 shows insertion
120 points and the paths of the eight hill-type muscles included in the base model, i.e., gluteus maximus
121 (GMAX), biarticular hamstrings (HAMS), iliopsoas (ILPSO), biarticular rectus femoris (RF), vasti (VAS),
122 biarticular gastrocnemius (GAS), soleus (SOL), and tibialis anterior (TA). Table 1 lists the maximum
123 isometric strengths for the muscles included in the base model along with the acronyms. At the beginning
124 of the simulation, the muscle states were set by equilibrating the muscle and tendon forces with the default
125 muscle activations of 0.05.

126 The chair-body contact interactions were modelled using a point on point kinematic constraint between
127 the femur head and the chair. During simulation, the kinematic constraint was disabled when the vertical
128 reaction forces required to maintain it turned non-compressive or if the slipping condition was satisfied.
129 The seat kinematic constraint, once disabled, could not be re-engaged and thus prevented optimization
130 from getting stuck into local optima with multiple chair rises. The model has nonlinear torsional springs,
131 representing ligaments at hip, knee, and ankle joints to limit the motion to a physiologically plausible
132 range. They generate torques when the hip joint flex beyond 120° or extends below 30° , or the knee joint
133 flex beyond 140° or extend beyond 0° , or the ankle dorsiflex beyond 30° or plantarflex beyond 40° . The
134 limits above whom the torsional springs generate are from the source model while the torsional spring
135 parameters are from Ong et al. (2019).

136 External assistance was introduced at the torso's COM in the musculoskeletal model that failed to perform
137 unaided STS transition. The rationale behind introducing it at the torso is explained in subsection 3.3. The
138 external assistance was modelled using two independent point forces acting in the vertical and horizontal
139 directions for the reasons of implementation simplicity. Their respective magnitudes were limited to the
140 0-200 N range. Before computing actuation, the excitation signals to point forces were passed through
141 first-order activation dynamics. The first-order activation dynamics (Millard, 1999) is the same as those
142 of the hill-type muscle present within the musculoskeletal models and had a time constant of 0.1 sec. It
143 made the assistance trajectories smoother and thus helped the optimization algorithm. The OpenSim API
144 (Delp et al., 2007) was used to formulate the musculoskeletal model's equation of motion and their forward
145 integration.

146 2.2 Optimization Setup

147 Our optimization framework tuned the values of nodes points obtained by discretizing the excitation
148 trajectories of the actuators present within the musculoskeletal model, i.e., muscles and external assistance
149 and the simulation duration (t_f). Piecewise linear functions were used for this discretization. The time
150 difference between the consecutive node points had a fixed value of 0.1 sec. The upper limit of simulation
151 duration (t_{max}) was 1.6 sec, similar to Yokota et al. (2016). All the musculoskeletal models had 8 hill-type
152 muscles. The externally assisted musculoskeletal model had two additional actuators, i.e., 2 point force
153 representing the external assistance. At t_0 , the actuators had their default activation. Thus, the optimization
154 problem had 129 decision variables when generating unaided STS trajectories and 161 decision variables
155 when generating assisted STS trajectories.

156 As mentioned before, aCMA-ES is a stochastic gradient-free optimization algorithm that adapts a
 157 Gaussian distribution towards low energy regions. Five restarts were performed to account for the
 158 stochasticity and non-linearity optimization space before selecting the optimal trajectory among them. The
 159 covariance matrix was reset at each restart, and the best-seen candidate till then was used as the mean. The
 160 excitation values corresponding to the model sitting in the chair were used as the initial guess for the mean.
 161 A restart was performed if the number of generations exceeded 4000 or if the improvement in the cost
 162 function value of the generation-wise best candidate solution in the last 250 generations was less than 1.0.
 163 We used the *libcmaes* library (CMA-ES, 2013) for the aCMA-ES algorithm.

164 2.3 Cost Function

165 The cost function we selected to engender STS transition is a linear combination of ten different terms
 166 and can be expressed as follows:

$$\phi_{total} = \sum_{i=1}^{10} w_i \phi_i \quad (1)$$

167 where w_i is the relative weight of i^{th} cost term, i.e., ϕ_i . The mathematical expressions for the ten cost
 168 terms are given in eqs. 2 - 12. Please refer to Table 2 for the list of symbols used in these equations. The w_i
 169 values were determined heuristically and are listed in Table 3. All the elements associated with different
 170 costs were computed in SI units.

$$\phi_1 = \frac{d(C_f, C_{goal})}{d(C_0, C_{goal})} \quad (2)$$

$$\phi_2 = [1 - \alpha] \int_{t_0}^{t_f} \frac{e^{t/\tau}}{\tau[e^{t_f/\tau} - 1]} F_{chair,y}(t) dt \quad (3)$$

$$\phi_3 = \sqrt{\frac{\sum_i \int_{t_0}^{t_f} a_i(t)^2 dt}{\sum i}} \quad (4)$$

$$\phi_4 = \sqrt{\frac{\sum_i \int_{t_0}^{t_f} \dot{a}_i(t)^2 dt}{\sum i}} \quad (5)$$

$$\phi_5 = \int_{t_0}^{t_f} \|F_{Assist}(t)\| dt \quad (6)$$

$$\phi_6 = \sum_n \int_{t_0}^{t_f} |T_{n,limit}(t)| dt \quad (7)$$

$$\phi_7 = \alpha \max_{\{t_0, t_f\}} (0, |F_{feet,x}(t)| - \mu F_{feet,y}(t)) \quad (8)$$

$$\phi_8 = \alpha \max_{\{t_0, t_f\}} |ZMP_x(t) - Feet_x(t)| dt \quad (9)$$

$$\phi_9 = \alpha \left[|\dot{\theta}_{hip}(t_f)| + |\dot{\theta}_{knee}(t_f)| + |\dot{\theta}_{ankle}(t_f)| \right] \quad (10)$$

$$\phi_{10} = \alpha \left[\begin{array}{l} \max_{\{t_{SR}, t_f\}} (F_{feet,y}(t)) - mg \\ \min_{\{t_{SR}, t_f\}} (F_{feet,y}(t)) - mg \\ |(F_{feet,y}(t_f)) - mg| \end{array} \right] \quad (11)$$

$$\alpha = 1 - \frac{\min(d(C_f, C_{goal}), d(C_0, C_{goal}))}{d(C_0, C_{goal})} \quad (12)$$

171 Cost ϕ_1 is the ratio of euclidean distances between the goal and t_f COM positions, and the goal and t_0
 172 COM positions. The goal COM position corresponds to the model standing upright. Cost ϕ_2 penalizes the
 173 model staying in contact with the chair during the later simulation parts. Costs ϕ_1 and ϕ_2 combined leads
 174 the model out of the chair, towards the standing posture (Figure 4). Costs ϕ_3 and ϕ_4 penalize the control
 175 effort and its rate of change, respectively. Cost ϕ_5 demotivates excessive use of external assistance. It was
 176 set to zero for the unassisted STS trajectories. Cost ϕ_6 discourages hyper-flexion and hyper-extension of
 177 joints. Costs ϕ_7 and ϕ_8 penalize the feet contact forces that would lead to slip or tipping over the toes or
 178 heel, respectively. Cost ϕ_9 penalizes the body motion at t_f while cost ϕ_{10} penalizes the excessive body
 179 accelerations.

180 Figure 3, illustrates the scalar α that represents STS progress. During the initial generations, the COM
 181 position at t_f is far away from standing posture COM, hence the value of α is zero (Figure 4). Then as the
 182 optimization progresses, the model learns to get off from the chair, i.e., C_f moves towards C_{goal} , and α
 183 approaches 1. While learning successful STS, the optimization first comes across unstable STS trajectories.
 184 Costs ϕ_7 to ϕ_{10} are scaled with α to prevent them from hindering the successful exploration of stable STS
 185 trajectories through the unstable ones. Cost term ϕ_2 is scaled by $(1 - \alpha)$ to reduce its relative contributions
 186 to the total cost during the later optimization stages.

187 2.4 Motion Tracking Setup

188 The OpenSim CMC tool-based motion tracking was used to investigate the failure of STS in this study.
 189 The CMC tool computes the actuator excitation levels at user-specified time intervals that will drive the
 190 generalized coordinates (\vec{q}) of the musculoskeletal model towards a desired kinematic trajectory (\vec{q}_{exp}) in
 191 the presence of external forces. At any given time t , the CMC tool first computes the desired acceleration
 192 $\ddot{\vec{q}}^*$ using the following proportional derivative control law:

$$\ddot{\vec{q}}^*(t + T) = \ddot{\vec{q}}_{exp}(t + T) + \vec{k}_v [\dot{\vec{q}}_{exp}(t) - \dot{\vec{q}}(t)] + \vec{k}_p [\vec{q}_{exp}(t) - \vec{q}(t)] \quad (13)$$

193 where, \vec{k}_v and \vec{k}_p are the feedback gains on the velocity and position errors, respectively. Since the
 194 forces that muscles apply cannot change instantaneously, the desired accelerations are computed some
 195 small-time T in the future. Then, CMC tool uses static optimization to distribute the load across synergistic
 196 actuators using static optimization. CMC tool offers two formulations for static optimization referred to as
 197 slow target and fast target. We used the fast target formulation. It minimizes the sum of squared controls
 198 augmented by a set of equality constraints which can be mathematically represented as follows:

$$J = \sum_{i=1} e_i^2 \quad (14)$$

$$C_j = \ddot{q}_j^* - \ddot{q}_j \quad \forall j \quad (15)$$

199 where e_i is the control input/excitation of i^{th} actuator at time t and q_j is the j^{th} generalized coordinate.
 200 Since for many \ddot{q}_j^* the muscles might not be able to produce sufficient forces, usually ideal torque actuators
 201 are added to the musculoskeletal model to prevent the fast target formulation from failing. Usually, the
 202 forces/torques produced per unit control effort for the ideal actuators is much lower than muscles. In
 203 such setups, following equation 14, ideal torque actuators produce significant force/torque only when the
 204 muscles are saturated, and hence they are also referred to as reserve actuators. Since the CMC tool does not
 205 support event detection based disabling of constraints, the seat contact force was supplied as an external
 206 force rather than a kinematic constraint. The seat force was pre-computed for the target STS trajectory
 207 before running the CMC tool.

208 2.5 Experimental Data Processing

209 We have used the experimental data recordings of Lao et al. (2019) and Lao et al. (2020) to validate the
 210 optimal STS trajectory generated 0% strength deficit model. The experimental data consists of optical
 211 marker data, surface EMG data and the ground and seat-pan reaction forces for 12 healthy adult subjects
 212 performing assisted and unassisted STS. Since the experimental data don't contain functional trials needed
 213 for musculoskeletal model scaling, we have used the trials of only a single subject with weight and height
 214 closest to our model. The selected subject weighs 71Kg and is 169cm tall. The source musculoskeletal
 215 model is of an adult male of mass 75Kg and height 170cm.

216 The unassisted STS trajectories consisted of 6 trials under four different conditions, i.e., arms folded
 217 across chest, arms hanging freely next to the body, natural STS, and slow pace imitating assisted
 218 STS. The 18 recordings belonging to the first three categories were by us. The optical markers on the
 219 musculoskeletal model were placed in the average optical marker positions recorded during the T-pose trial.
 220 This musculoskeletal model with registered optical markers was used for performing inverse kinematics.
 221 We defined the beginning and the end of STS as the times when hip flexion and hip extensions velocities
 222 smoothed with a rolling window of 0.1s were respectively higher or lower than 20°/s. Figure 5 compares
 223 the mean initial postures recorded in experiments and the initial posture used to generate STS trajectories.
 224 The model was moved slightly forward towards the feet for simulations to compensate for the non-actuated
 225 lumbar joint. Also, the simulation's initial posture should be easier to stand up from due to the torso lying
 226 closer to the feet.

227 The sEMG data was processed by first passing through a fourth-order Butterworth bandpass filter with
 228 cutoff frequencies of 10Hz and 350Hz. Then it was rectified and subsequently passed through a fourth-order
 229 Butterworth lowpass filter with a cutoff frequency of 3Hz. The sEMG data for STS trials was normalized
 230 using the maximum values recorded during the maximum voluntary control trials.

3 RESULTS

231 The optimization could generate successful STS trajectories for the 0%, 20%, 40% and 60% strength deficit
 232 models. However, for the 80% strength deficit model, the optimization framework could only generate a
 233 successful STS trajectory when the model was assisted externally at the torso. For conciseness, we refer to
 234 these trajectories as those of the models even though the models were only one component of the complete
 235 optimization framework. The STS trajectories are divided into three phases as suggested in Millington
 236 et al. (1992) to facilitate discussions. Phase 1 starts with the trunk flexion and ends when the model loses
 237 contact with the chair. Phase 2 starts with the knee extension and ends when the hip joint is maximally

flexed. Phase 3 begins with the reversal of trunk flexion to extension and ends with the model standing upright. The vertical black dotted lines in Figures 6-12 marks the transition between the three phases.

The results are organized into three subsections. In subsection 3.1 first, the STS trajectory of the 0% strength deficit model is contrasted against those of a healthy adult validation, and then its kinematics and dynamics are detailed. In subsection 3.2, first, the adaptations caused by muscle strength deficits are reported, and then they along with motion-tracking results are used to suggest an explanation for the failure of optimization to generate STS using the 80% strength deficit model. In subsection 3.3, the features of the STS trajectory generated using the externally assisted 60% strength deficit model are discussed. Please refer to Figures 6-11 and Table 4 during the following subsections for details. The resultant joint torques, in Figure 11 and Table 4, were obtained using inverse dynamical analysis of the STS trajectories using OpenSimDelp et al. (2007). During inverse dynamical analysis, the muscles forces were excluded, while the seat constraint and assistance forces were supplied as external forces. The contributions of muscle forces to the resultant joint torques were computed using the Muscle Analysis tool of OpenSim.

3.1 Unassisted STS Trajectory of 0% Strength Deficit Model

Figures 6 to 10 respectively illustrates the joint angle, the muscle excitation, the COM position and velocity, feet force zero moment point (*ZMP*), and the contact force trajectories associated with the optimal STS trajectory generated using the 0% strength deficit model. The STS motion is initiated by activating the ILPSO and RF muscles (Figure 7). Their activation generates torque around the hip joint and flexes the torso forward (Figure 11). It is followed by the deactivation of ILPSO and RF muscles and gradually increasing activations of the GMAX and HAMS muscles. Due to the trunk's forward flexion, the COM's horizontal velocity increases and peaks as the activations of the GMAX and HAMS muscles increase to control the torso's forward flexion. Also, the activation of VAS muscle increases to prepare for seat-off. Phase 1 ends when the VAS muscle has generated sufficient torques around the knee joint to lift the musculoskeletal model off the chair. The seat off takes place with the body's COM lying behind ZMP computed using feet forces (Figure 9). During phase 2, the GMAX and HAMS muscle activations increase until the hip flexion velocity reduces to zero. At this point, the trunk is maximally flexed, phase 2 comes to an end. The knee joint extends only slightly during phase 2. The peak VAS, GMAZ and HAMS muscle activations occur during phase 2. During phase 3, the activation of GMAX, HAMS, and VAS muscles slowly taper off as smaller forces are required to continue standing up since an increasing fraction of body weight is borne by bone alignment. These patterns lead to the extension of both the hip and knee joints until the standing posture is achieved. At the end of phase 3, increased activation is observed in ILPSO, RF, and TA muscles to stop the hip, knee and ankle joints from extending past the upright posture. Also, during the latter half of phase 3, the body's COM reaches the feet support polygon. Significant TA muscle activations are present during all three phases. During the first two phases and a significant part of the third phase, the TA activation counteracts the passive fiber forces of the SOL muscles. These activations produce the force needed to balance the counteracting SOL and GAS muscle forces. The SOL muscles see almost negligible activation throughout the three phases.

The joint angle trajectories of 0% strength deficits are contrasted against those observed experimentally for a healthy adult in Figure 6 (B). The general shape of the hip and knee joint angle trajectories matches those of experiments. The discrepancies in the joint angle trajectories primarily result from the different initial postures (Figure 5). The mean initial posture from experiments requires the lumbar joint extension from -30° to nearly 0° . Our model did not include lumbar joint actuation for the reasons of modelling simplification. The initial posture was modified to compensate for the non-actuated lumbar joint by moving the model slightly forward and locking the lumbar joint with 10° of flexion.

282 The muscle activation patterns of the 0% strength deficit model are compared to those of experiments
 283 in Figure 7. The general shape of the critical muscles for STS, i.e., GMAX, HAMS and VAS, matches
 284 those of experiments. The higher activation of VAS than experiments during the first half of phase 1 is
 285 most potentially due to cost term ϕ_2 . Muscle RF features higher activation during the beginning of STS as
 286 the model didn't feature trunk muscles to initiate motion. The higher activation of TA than experiments is
 287 most potentially due to the passive fiber forces induced in SOL muscle due to initial posture. Experimental
 288 data features a small peak in the TA, GAS and SOL muscle activations during phase 2. This peak is absent
 289 in the generated STS. The experimental data did not include EMG signal for ILPSO muscle. Their peak
 290 activations of all the muscles are within the two standard deviations of the peaks observed in experiments
 291 except for RF and TA muscle.

292 The seat and feet contact forces trajectories for the STS motion of the 0% strength deficit model are
 293 compared to those observed in experiments in Figure 10. The lower seat-pan forces are most potentially
 294 because of the point on point constraint-based formulation. The flattening in the peak feet forces for
 295 simulation is because of the cost term ϕ_{10} . Also, the seat-off in simulation occurs before then in the
 296 experiments. It is potentially because of reduced horizontal momentum required due to initial posture and
 297 the simpler seat constraint formulation, making it easier to develop horizontal momentum.

298 3.2 STS Adaptation and Failure

299 With strength deficits, the STS duration and the peak activation of VAS, GMAX, RF, ILPSO and TA
 300 muscles increases (4 and Figure 11). The peak activation of HAMS increases with strength deficits until
 301 the model with the 40% strength deficit model's STS trajectory. For the 60% strength deficit model's STS
 302 trajectory, a decrease in peak activation of HAMS muscle is observed compared to the 40% strength deficit
 303 model. The peak activation of VAS muscle is higher than those of GMAX and HAMS muscles for the STS
 304 trajectories of models up to 40% strength deficits. The decrease in the peak activation of HAMS muscle
 305 for the 60% strength deficit model's STS trajectory is to alleviate the saturated antagonistic VAS muscle
 306 across the knee joint. It is evident from the contribution of HAMS to peak resultant knee torques dropping
 307 from -112.17% for the 40% strength deficit model -30.99% for the 60% strength deficit model. The
 308 reduced activation of HAMS muscle saturates the GMAX muscle as they work in conjunction to control
 309 the hip flexion. It is demonstrated by the contributions of HAMS muscle to the peak resultant hip torques
 310 dropping from 70.26% for the 40% strength deficit models to 54.7% for the 60% strength deficit model.
 311 Also, a reduction in peak COM velocity, ground reaction forces, and GMAX, HAMS and VAS muscle
 312 forces is observed from the 40% strength deficit model's to 60% strength deficit model's STS trajectory.
 313 Bobbert et al. (2016) also observes that with strength deficits, the STS duration increases, while the peak
 314 COM vertical velocity, peak GMAX, and VAS muscle forces decrease. However, Bobbert et al. (2016)
 315 does not observe a significant reduction in HAMS muscle activation. It is potentially because Bobbert et al.
 316 (2016) used the solution of the previous optimal trajectory as the initial for the following optimization
 317 problem. Besides STS duration and muscle activation, we do not observe any consistent trend between the
 318 0% strength deficit to 40% strength deficit STS trajectory. It is most potentially because the optimization
 319 was converging to a different local optimum for each model.

320 The optimization framework failed to generate the STS transition for the 80% strength deficit model. We
 321 suspected the GMAX or the VAS muscle to be responsible for this failure as they were getting saturated
 322 during the STS trajectory of the 60% strength deficit model (Figure 11). We used the 80% strength deficit
 323 model and OpenSim CMC Tool to track the successful STS motion of 60% strength deficit. Two different
 324 setups of reserve actuators were used to aid the muscles. In the first setup, the optimal torque, i.e., torques
 325 generated per unit control effort, for the hip and knee torque actuators were 100Nm and 1Nm respectively,

326 while in the second setup, they were $1Nm$ and $100Nm$. The first setup favored the utilization of the hip
 327 reserve actuator, while the second setup favored the utilization of the knee reserve actuator. The first
 328 setup's motion-tracking features a peak torque of $-19.81Nm$ by the knee reserve actuator and increased
 329 activation of both VAS and RF muscles. The second setup-based motion-tracking features a peak torque of
 330 $-12.05Nm$ by the hip reserve actuator and increased HAMS and GMAX activations. The lower magnitude
 331 of reserve actuator in the second setup compared to the first supports the hypothesis that the failure to
 332 generate STS motion between the 60% to 80% strength deficits will occur because of VAS muscle weakness.
 333 The observation of higher or equal peak activation of VAS muscle to GMAX for all the model's also
 334 supports this hypothesis.

335 3.3 Externally Assisted STS transition

336 It was observed in the last subsection that assisting the musculoskeletal model primarily at the hip joint
 337 leads to increased RF muscle activation, while assisting it primarily at the knee joint leads to increased
 338 HAMS muscle activation. As STS transition is performed several times a day, assisting only at the hip or
 339 the knee joint will lead to the contracture of the RF or the HAMS muscle, respectively. As both the muscles
 340 cross the hip joint in an antagonistic manner, their contracture has a high potential to lead to back pain
 341 issues. Thus the external assistance was introduced at the torso COM in the 80% strength deficit model.
 342 Also, assisting the model at the torso center of mass is a good approximation for assisting a human at the
 343 underarms area. The underarms area is easily graspable, and assistance using it helps simplify the design of
 344 a probable STS assistance device.

345 When provided in an assist-as-needed manner, physical assistance can help maintain or recover lower
 346 extremity strength. Thus while generating the assisted STS trajectories, the over-utilization of external
 347 assistance was penalized (Equation 6). Figure 12 shows the body postures, the assistance forces, and muscle
 348 activation for the optimal STS trajectory generated using the externally assisted 80% strength deficit model.
 349 The STS trajectory features utilization of external assistance only when the VAS and GMAX muscle starts
 350 getting saturated, i.e., it uses external assistance only when needed. The peak magnitudes of external
 351 assistance's vertical and horizontal components are 36.50% and 44.51% of body weight, respectively. The
 352 STS trajectory features reduced peak com velocities, net hip and knee joint torques and the VAS, GMAX,
 353 and HAMS muscle forces. The seat-off takes place with the torso in a more upright posture compared to
 354 unassisted models.

4 DISCUSSION

355 This paper presented and analyzed the STS trajectories generated using open-loop single shooting
 356 optimization for musculoskeletal models with different muscle strength deficit levels. The strength deficits
 357 were introduced by scaling the maximum isometric strength of all the muscles in steps of 20%. The strength deficits
 358 could successfully generate STS trajectories for models with up to 60% strength deficits.
 359 The common muscle activation patterns for the 0% strength deficit model agree with the experimental
 360 observations for a healthy subject. As muscle strength deficit increased, the simulation duration increased.
 361 When the VAS muscle got saturated (60% strength deficit model), a reduction in the activation of the
 362 antagonistic HAMS muscle to alleviate it was observed. The reduced HAMS muscle activation led to
 363 increased GMAX muscle activation. Then the motion-tracking results were used to propose the VAS
 364 muscle weakness as the reason for optimization's failure to generate an STS trajectory. The motion tracking
 365 results were also used to motivate the introduction of external assistance at torso COM. Optimization
 366 was able to generate a successful STS trajectory for the externally assisted 80% strength deficit model.
 367 The trajectory featured the usage of external assistance in an assist-as-needed manner. After experimental

validation with elderly adults in future, observing reduced HAMS activation compared to GMAX muscle may help plan intervention. We also showed the optimization framework's capability to generate externally assisted trajectories. We make the source code of optimization to speed up the design of assist-as-needed STS devices. The findings of this study should be observed with caution as it they have many inherent assumptions. The most significant known assumptions are discussed in the next few paragraphs followed by our future research directions.

Many experimental studies report that some elderly follow a stabilization strategy in which they move the COM over feet support polygon before losing contact with the chair. Like the initial posture of our experiments, the stabilization strategy requires significant lumbar motion. Also, for the sitting posture with maximum trunk flexion (120°), the COM lies just 1.15cm inside the feet support polygon. Thus the elimination of lumbar joint and fixed feet position relative to the chair, even though also made by Pandy et al. (1995), Bobbert et al. (2016), and Yokota et al. (2016), might be an oversimplification for generating STS trajectories of elderly adults.

Strength deficits were introduced by simultaneously scaling all the muscles' maximum isometric strength. Bobbert et al. (2016) and Yokota et al. (2016) also introduced strength deficits in a similar manner. However, the strength of all muscles does not deteriorate by the same ratio. Also, scaling the maximum isometric forces is not the only way to introduce strength deficits. For example, the peak muscle activations could have been limited to the same effect. We assumed a sagittal plane of symmetry. However, it has been shown that even for healthy adults, one leg is usually more dominant than the other. Also, asymmetries may arise when one of the upper extremities grabs surfaces for assistance. Thus, the optimization framework needs to be extended to use the 3D musculoskeletal model to generate more realistic assisted and unassisted STS trajectories. Other musculoskeletal model-related critical assumptions might be simplifying muscle groups to single musculotendon units and control level decoupling between muscles.

We assumed perfect coordination between the musculoskeletal model and external assistance leading to assisted STS transition in 1.11s . The optimization framework should be extended to include sensory noise and delay in external assistance to correctly represent real-life assisted STS, which is usually of much longer duration. The maximum simulation duration was limited to 1.6s and might have prevented the search of successful STS trajectories. Also, chair height plays an important role for STS, and the results of this study are a function of it.

The cost function used in this study is not unique in its capability to engender STS. Further, even for the selected cost function, the relative weights of the different cost terms should have been chosen using inverse optimal control. The relative weights were heuristically selected because of the computationally demanding nature of the optimization. The generated STS trajectories are local optimal solutions of nonlinear non-convex optimizations. The optimization's failure to generate STS using the 80% strength deficit model might have been because of the optimization setup rather than muscle saturation.

In the future, we plan to use the results of this study to design a kinematic events-based closed-loop controller for STS transition. We also plan to investigate the torque and muscle actuated lumbar joint models so as to generate STS trajectories with more accurate joint kinematics and dynamics. Finally, we intend to extend the optimization framework to include sensory noise and delay for the realistic model of an assist-as-needed STS assistance device.

5 AUTHOR CONTRIBUTIONS

408 Conceptualization: VK, TY, and TS; Methodology: VK; Software: VK; Data Analysis: VK; Validation:
409 TS; Writing—original draft preparation: VK; Writing—review and editing: VK, TY, and TS; Funding
410 acquisition: TS; Resources: TY and TS; Supervision: TS

6 DATA AVAILABILITY STATEMENT

411 The optimization source code and the results from this study are available at <https://github.com/>
412 ShibataLab/PredictiveSTS.

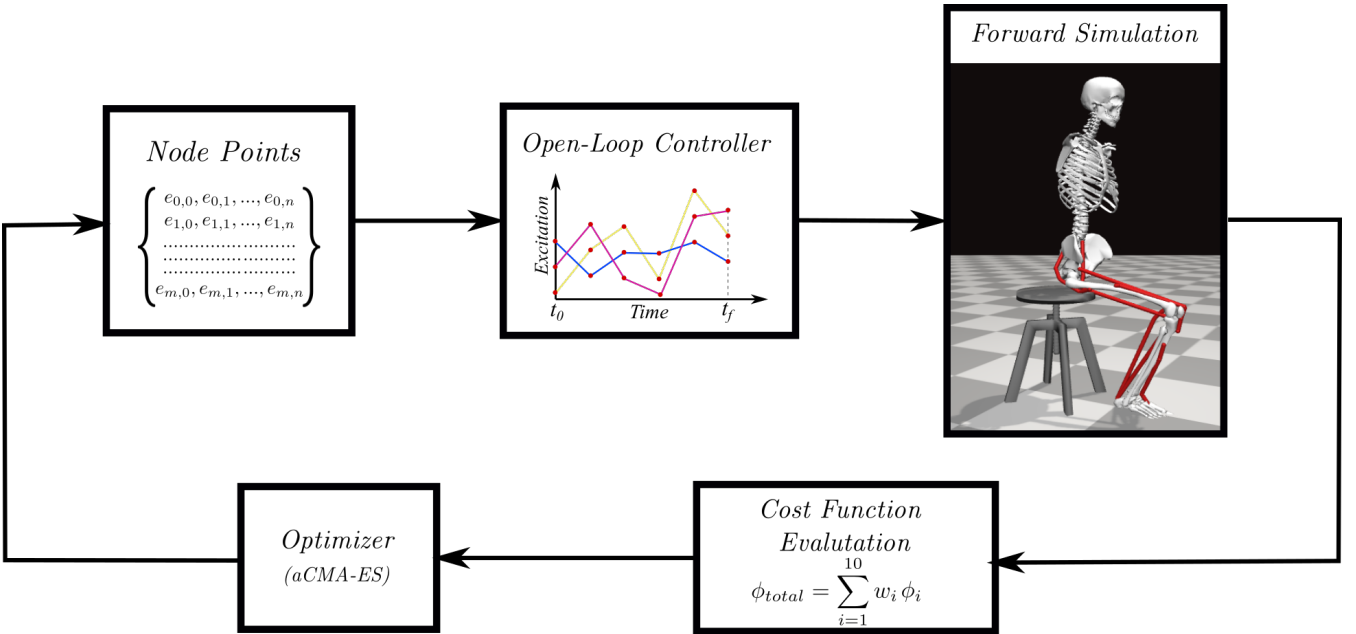


Figure 1. Overview of single shooting optimization framework. The red dots in the open-loop controller represents the node points obtained from the discretization of excitation trajectories.

Muscle	Acronym	Maximum Isometric Strength (N)
Iliopsoas	ILPSO	2697.3
Gluteus maximus	GMAX	3337.6
Biarticular Rectus Femoris	RF	2191.7
Biarticular Hamstrings	HAMS	4105.5
Vasti	VAS	9594.0
Biarticular Gastrocnemius	GAS	4690.6
Soleus	SOL	7925.0
Tibialis Anterior	TA	2116.8

Table 1. Muscles included in the model, their acronyms and their respective maximum isometric strengths for the 0% strength deficit model.

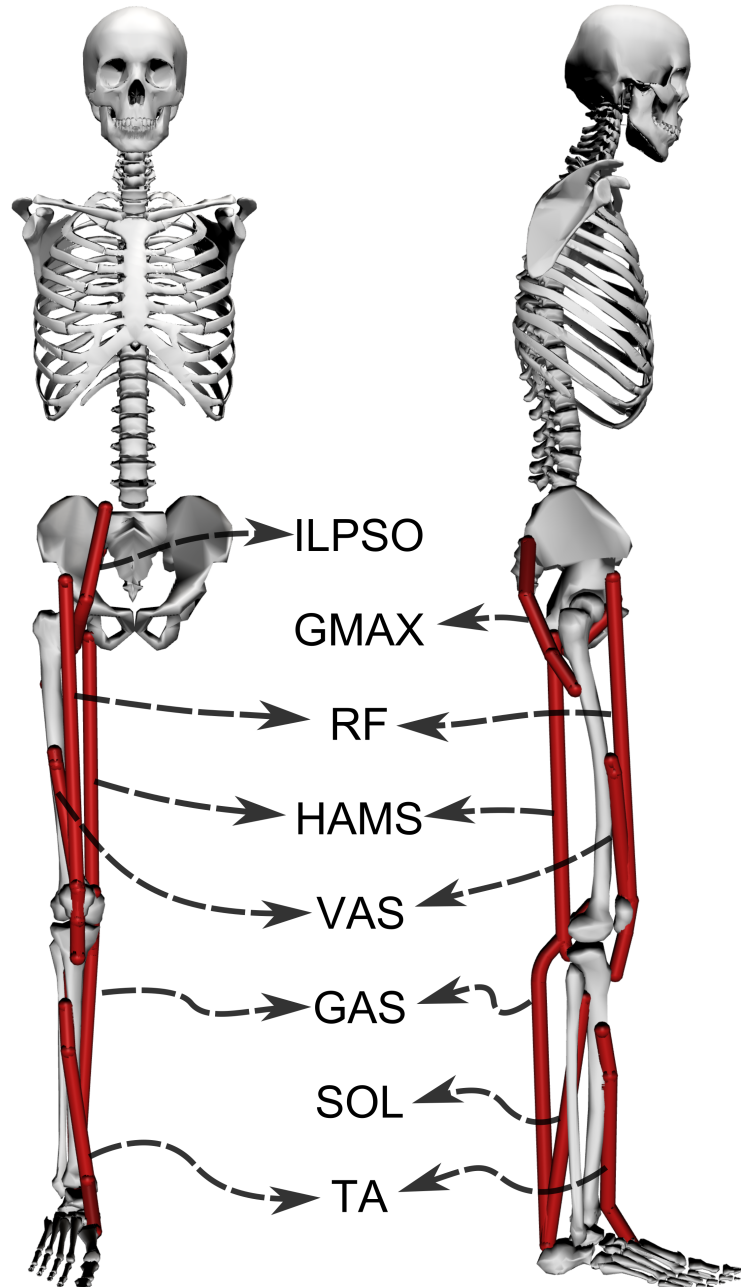


Figure 2. A planar musculoskeletal model for sit-to-stand. The model's musculotendon actuators (red lines) represents the major uniarticular and biarticular muscle groups that drive the sit-to-stand motion in the sagittal plane, i.e., iliopsoas (ILPSO), gluteus maximus (GMAX), biarticular rectus femoris (RF), biarticular hamstrings (HAMS), vasti (VAS), gastrocnemius (GAS), soleus (SOL), and tibialis anterior (TA). The model has three degrees of freedom distributed at the hip, knee and ankle joints.

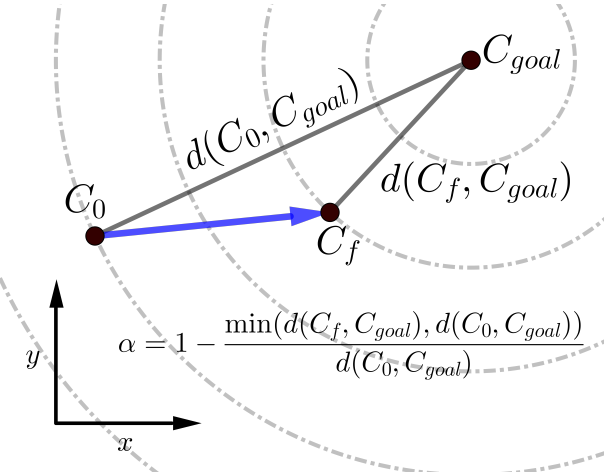


Figure 3. Scalar α , used within the cost expressions, represents the percentage of STS completion and ranges between 0 to 1. The dashed circles show the states that are equidistant from the C_{goal} .

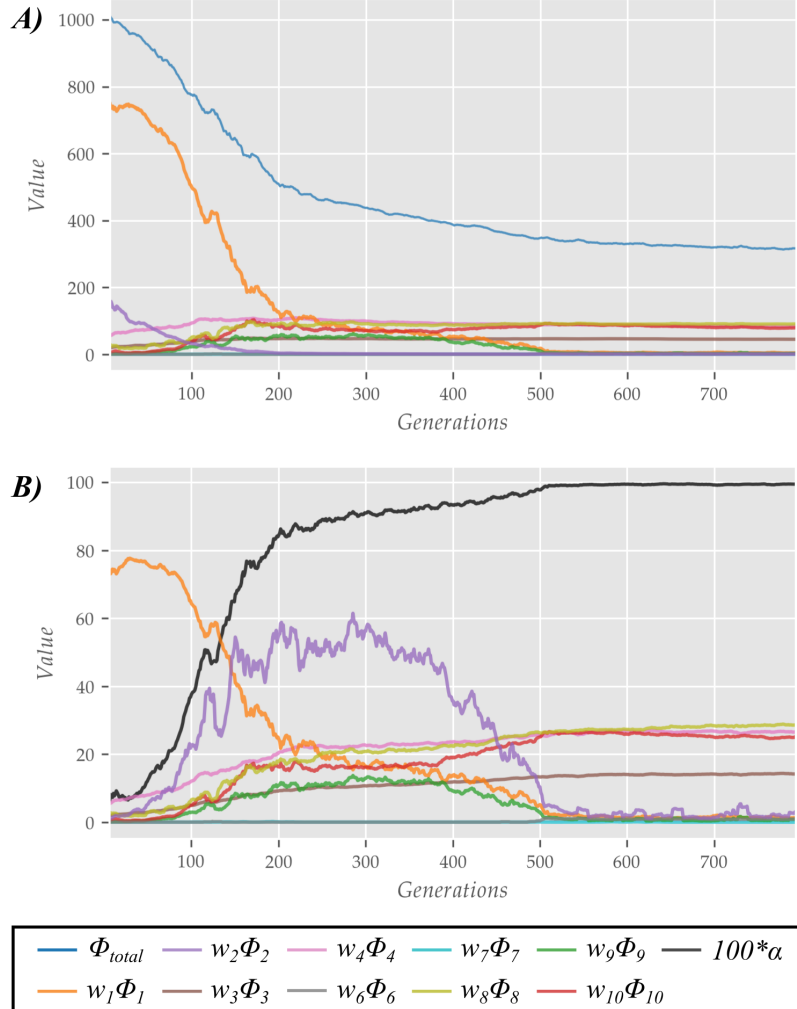


Figure 4. Evolution of different costs (**A**) and their relative contributions to the total cost (**B**) for the best candidates observed during trajectory optimization using the 0% strength deficit model. The costs were smoothed using a rolling average of 10 generations for this plot.

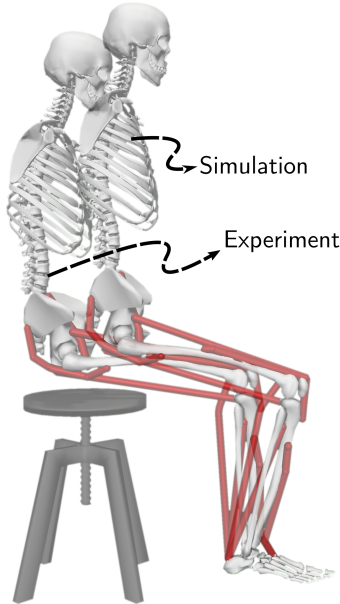


Figure 5. The initial posture used to generate STS trajectories and the mean initial posture observed during experiments. The model was moved slightly forward for simulation to compensate for its non-actuated lumbar joint.

Table 2. List of symbols.

Variable	Description
t	time
$\dots(t)$	Value of a expression .. at time t
$.. $	The absolute value expression ..
t_0	Simulation start time
t_f	Simulation final time
t_{max}	Upper limit of t_f
t_{SR}	Time of seat release
C_0	Center of mass at t_0
C_f	Center of mass at t_f
C_{goal}	Center of mass for standing posture
$d(C_1, C_2)$	Euclidean distance between center of mass positions at t_1 and t_2
α	% Sit to stand completion
$F_{chair,y}$	y component of constraint force applied by the chair on the femur head
τ	Time constant
a_i	Activation of actuator i
$ F_{Assist} $	Magnitude of external assistance
$T_{n,limit}$	Torque generated by the torsional limit spring at the n^{th} joint
$F_{feet,n}$	Component of force applied along n direction by the ground on the feet
ZMP_x	x coordinate of feet force zero moment point
$\dot{\theta}_j$	Velocity of joint j
$Feet_x$	x coordinate of the mid point between heel and toes
mg	Weight of musculoskeletal model

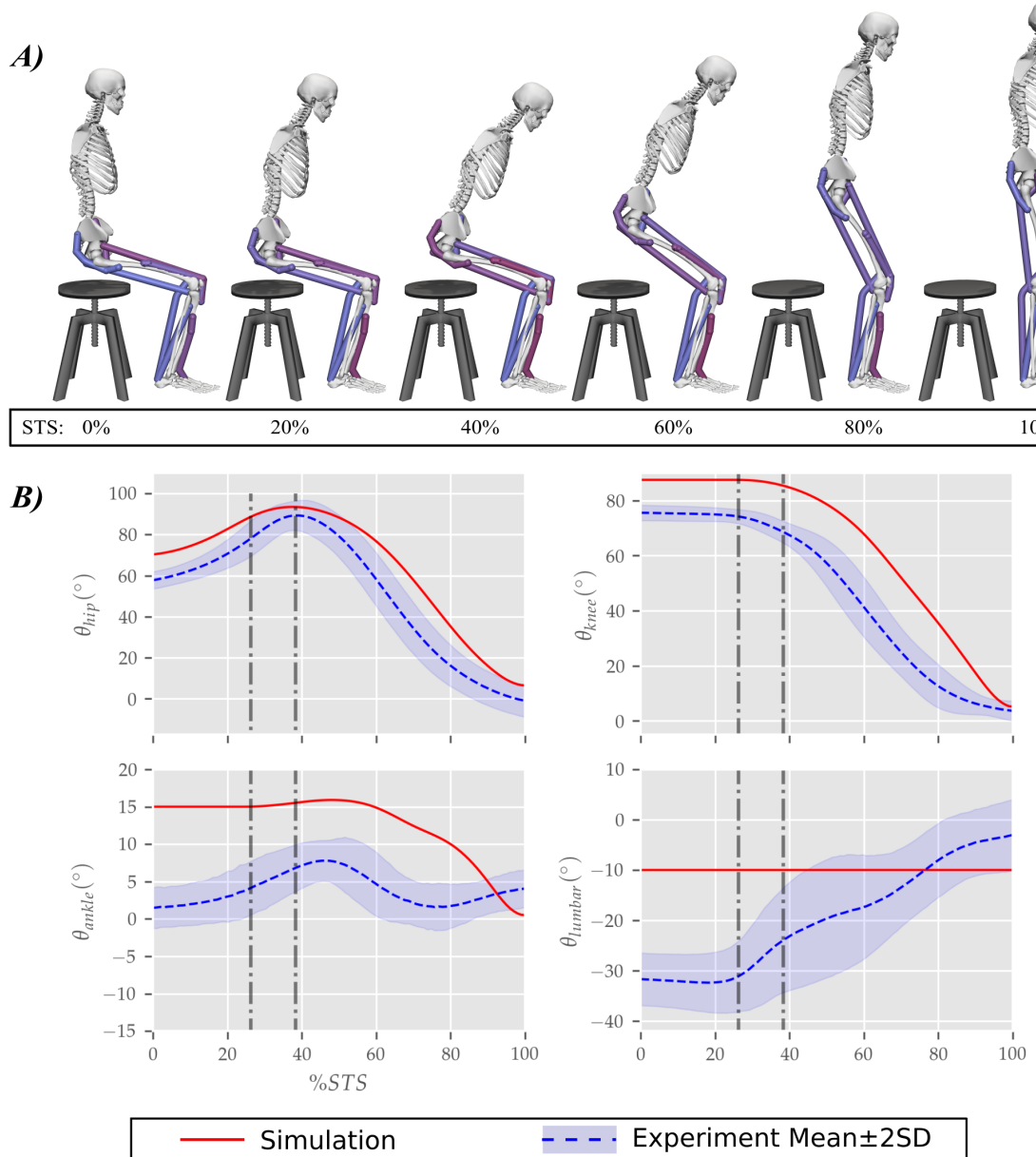


Figure 6. (A) Different postures observed during the STS transition of the 0% strength deficit model and the comparison of associated joint angle trajectories against experimental recordings (B). The first vertical dotted line marks the point when the model lost contact with the chair, and the second vertical dotted line marks the posture with maximum hip flexion.

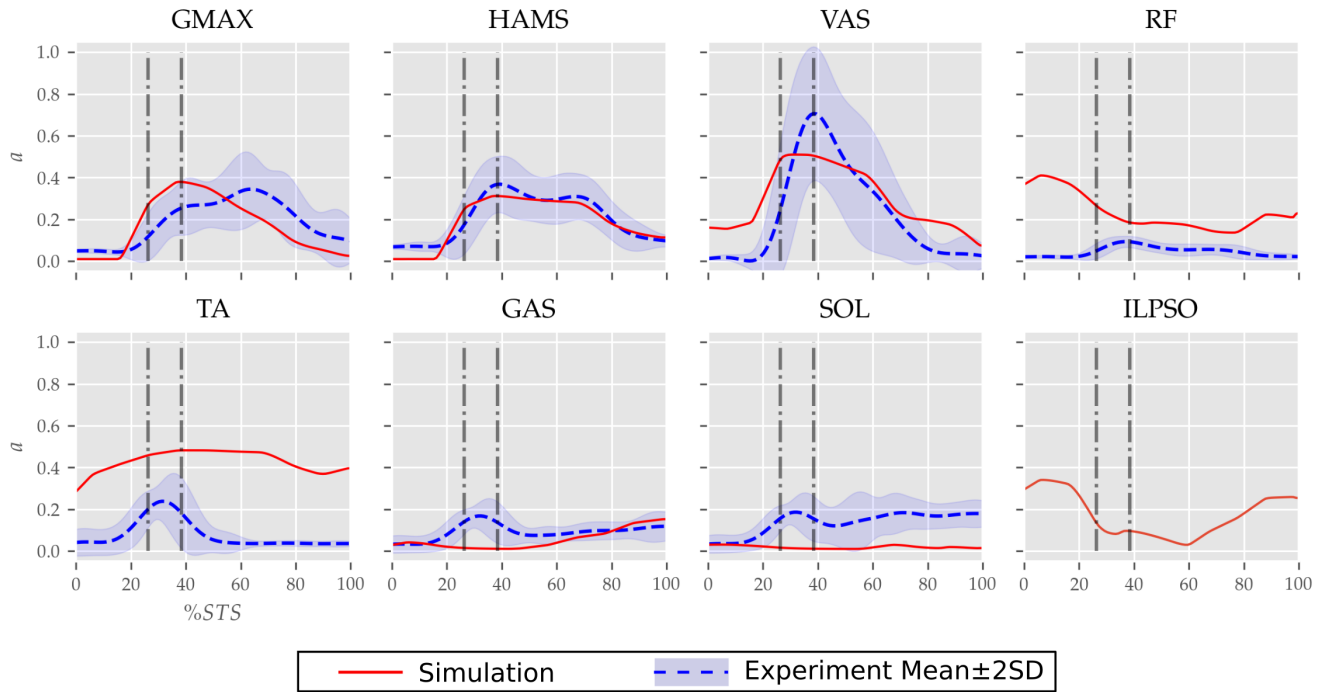


Figure 7. Muscle activation trajectories associated with the 0% strength deficit model's STS trajectory and those recorded experimentally.

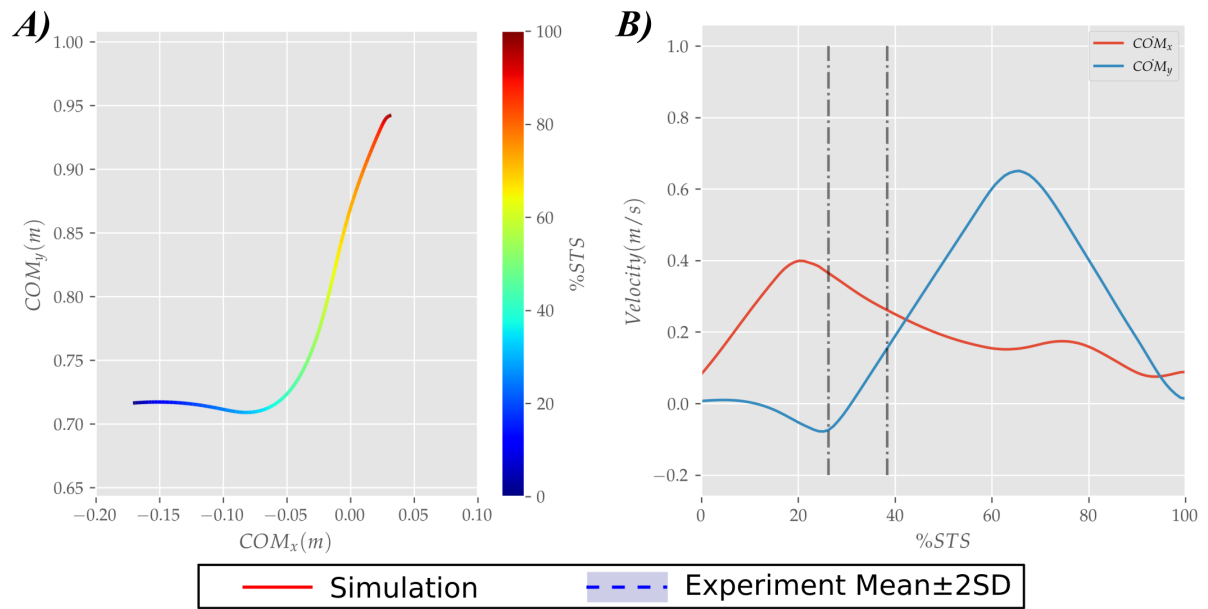


Figure 8. Evolution of COM position (**A**) and velocity (**B**) observed for the STS trajectory of 0% strength deficit model.

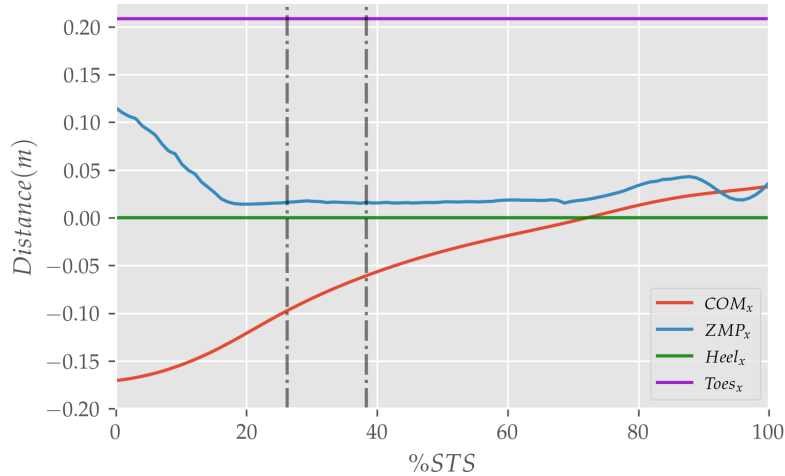


Figure 9. The zero moment point (feet forces) and the body's COM trajectories from the 0% strength deficit model's STS.

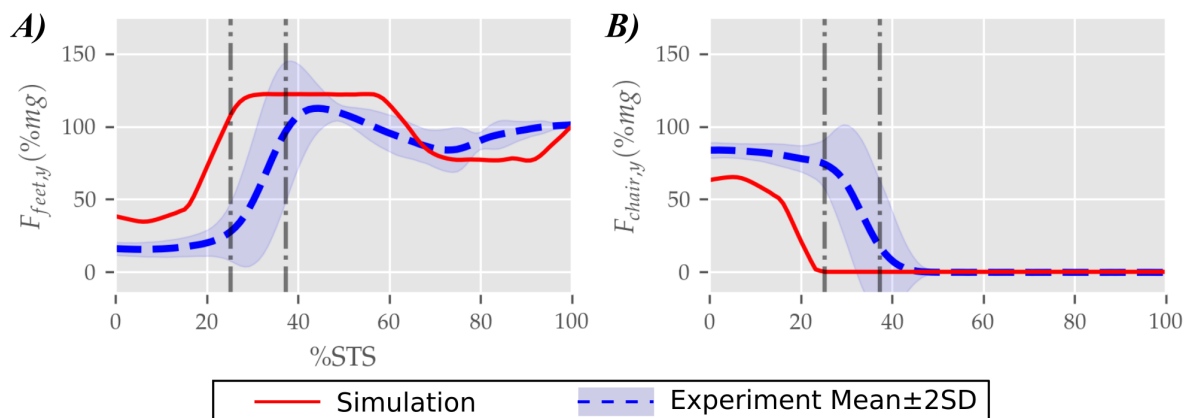


Figure 10. Feet (**A**) and seat contact forces (**B**) observed during the STS trajectory of the 0% strength deficit model and the experiments.

Table 3. Cost function hyperparameters.

Variable	Value
τ	$t_{max}/8$
w_1	800
w_2	1.2
w_3	175
w_4	70
w_5	5
w_6	10
w_7	0.1
w_8	1000
w_9	6
w_{10}	0.3

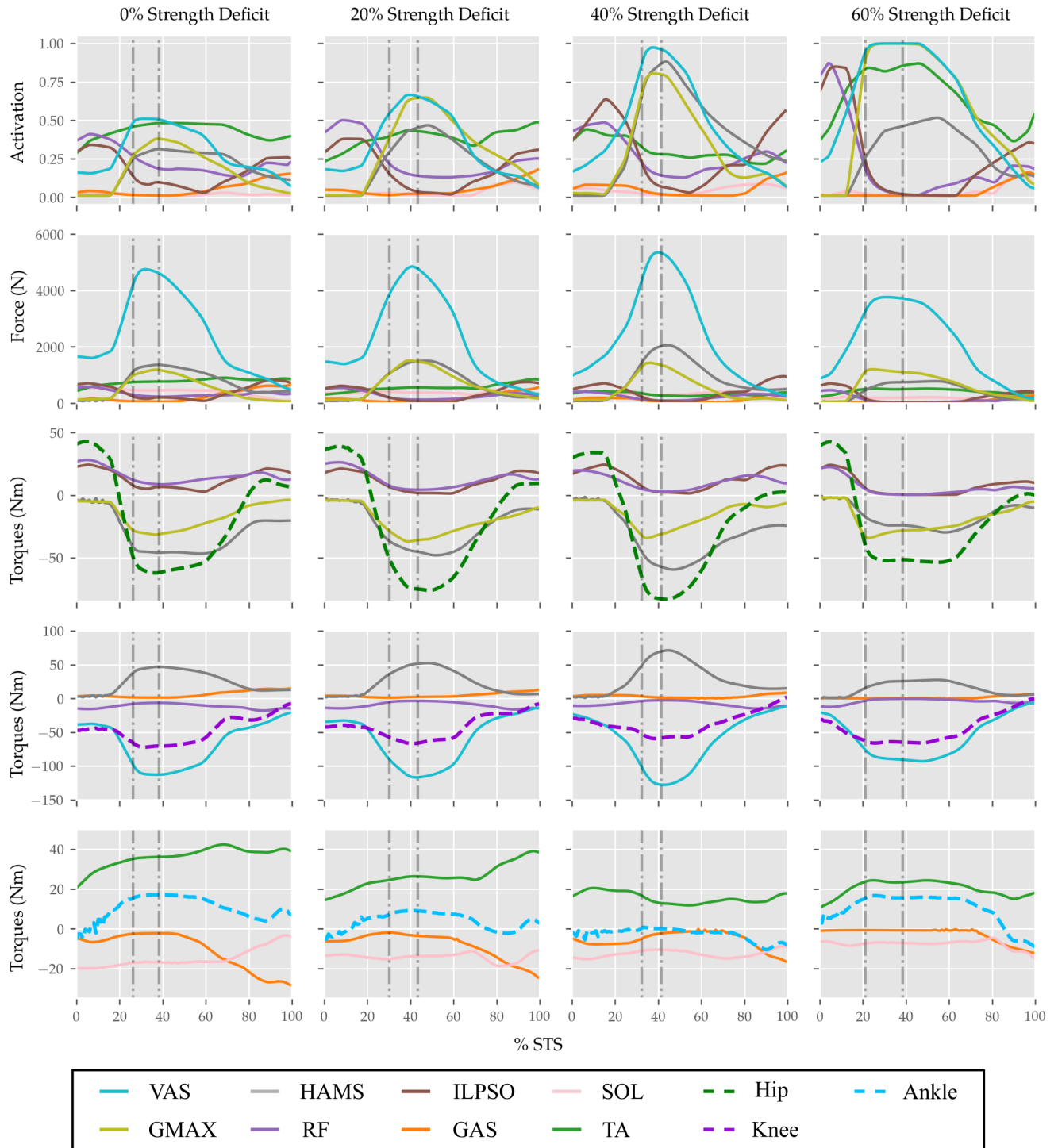


Figure 11. Muscle activations, muscle forces, and their respective contributions to the resultant joint torques from the STS trajectories of 0%, 20%, 40% and 60% strength deficit models.

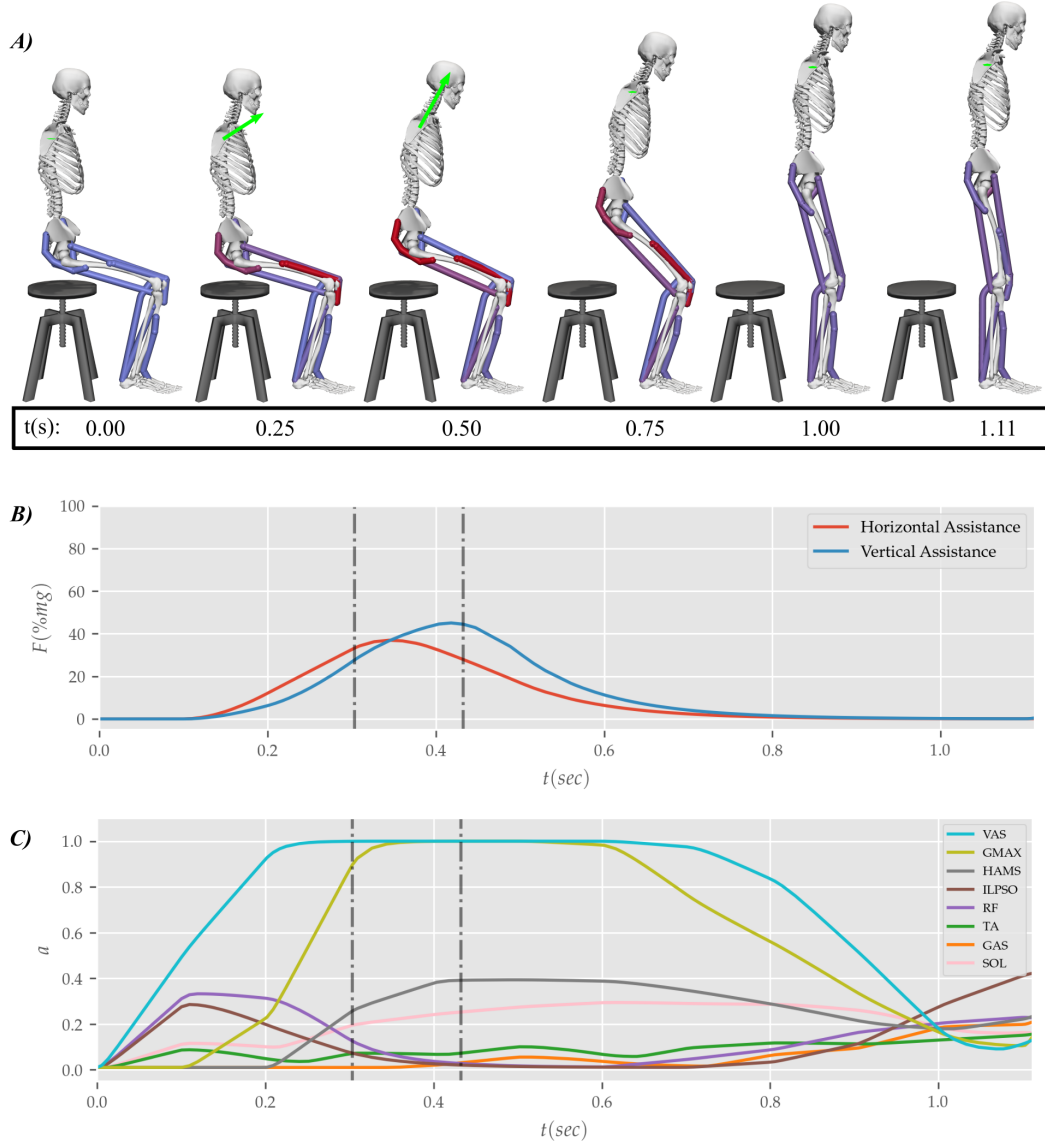


Figure 12. Postures (A) and the external assistance trajectories (B) from the STS transition of the externally assisted 80% strength deficit model. The green arrow in (A) represents the resultant external assistance force.

Table 4. Properties of the 0%, 20%, 40%, 60% and externally assisted 80% strength deficit model's STS trajectories. Rows 5, 6, 8 and 10 show contributions of muscles to peak resultant joint torques.

# Row	Property	0% Strength Deficit	20% Strength Deficit	40% Strength Deficit	60% Strength Deficit	80% Strength Deficit Assisted
1	STS duration (s)	1.14	1.23	1.33	1.47	1.11
2	Peak COM Horizontal Velocity (m/s)	0.40	0.42	0.42	0.39	0.43
3	Peak COM Vertical Velocity (m/s)	0.65	0.71	0.65	0.55	0.42
4	Peak Hip Torque (Nm)	-62.17	-76.10	-83.28	-53.58	-35.59
5	GMAX Peak Hip Torque (Nm)	-31.60	-35.12	-30.03	-26.17	-20.96
6	HAMS Peak Hip Torque (Nm)	-45.91	-47.15	-58.51	-29.31	-15.44
7	Peak Knee Torque (Nm)	-72.02	-66.73	-59.22	-65.86	-42.19
8	VAS Peak Knee Torque (Nm)	-111.26	-115.92	-125.02	-85.51	-42.36
9	HAMS Peak Knee Torque (Nm)	44.40	50.34	66.43	20.41	2.69
10	Peak VAS Force (N)	4754.10	4857.40	5355.19	3765.91	1907.14
11	Peak GMAX Force (N)	1194.27	1513.42	1437.11	1206.33	615.33
12	Peak HAMS Force (N)	1366.03	1505.99	2058.45	782.31	340.31

REFERENCES

- 413 Arnold, D. V. and Hansen, N. (2010). Active covariance matrix adaptation for the (1+ 1)-cma-es. In
414 *Proceedings of the 12th annual conference on Genetic and evolutionary computation*. 385–392
- 415 Bobbert, M. F., Kistemaker, D. A., Vaz, M. A., and Ackermann, M. (2016). Searching for strategies to
416 reduce the mechanical demands of the sit-to-stand task with a muscle-actuated optimal control model.
417 *Clinical Biomechanics* 37, 83–90
- 418 [Dataset] CMA-ES (2013). libcmaes. <https://github.com/CMA-ES/libcmaes>
- 419 Delp, S. L., Anderson, F. C., Arnold, A. S., Loan, P., Habib, A., John, C. T., et al. (2007). Opensim:
420 open-source software to create and analyze dynamic simulations of movement. *IEEE transactions on
421 biomedical engineering* 54, 1940–1950
- 422 Geravand, M., Korondi, P. Z., Werner, C., Hauer, K., and Peer, A. (2017). Human sit-to-stand transfer
423 modeling towards intuitive and biologically-inspired robot assistance. *Autonomous Robots* 41, 575–592
- 424 Hughes, M. A., Myers, B. S., and Schenkman, M. L. (1996). The role of strength in rising from a chair in
425 the functionally impaired elderly. *Journal of biomechanics* 29, 1509–1513
- 426 Lai, A. K., Arnold, A. S., and Wakeling, J. M. (2017). Why are antagonist muscles co-activated in my
427 simulation? a musculoskeletal model for analysing human locomotor tasks. *Annals of biomedical
428 engineering* 45, 2762–2774
- 429 Lao, B., Tamei, T., and Ikeda, K. (2019). Characterizing strategic contributions of physical therapy to
430 natural standing motion in the muscle synergy space. In *2019 41st Annual International Conference of
431 the IEEE Engineering in Medicine and Biology Society (EMBC)* (IEEE), 2311–2315
- 432 Lao, B., Tamei, T., and Ikeda, K. (2020). Data-efficient framework for personalized physiotherapy feedback.
433 *Frontiers in Computer Science* 2, 3
- 434 Lord, S. R., Murray, S. M., Chapman, K., Munro, B., and Tiedemann, A. (2002). Sit-to-stand performance
435 depends on sensation, speed, balance, and psychological status in addition to strength in older people.
436 *The Journals of Gerontology Series A: Biological Sciences and Medical Sciences* 57, M539–M543
- 437 Millard, M. (1999). First-order activation dynamics
- 438 Millington, P. J., Myklebust, B. M., and Shambes, G. M. (1992). Biomechanical analysis of the sit-to-stand
439 motion in elderly persons. *Archives of Physical Medicine and Rehabilitation* 73, 609–617
- 440 Mombaur, K. and Hoang, K.-L. H. (2017). How to best support sit to stand transfers of geriatric patients:
441 Motion optimization under external forces for the design of physical assistive devices. *Journal of
442 biomechanics* 58, 131–138
- 443 Norman-Gerum, V. and McPhee, J. (2018). Constrained dynamic optimization of sit-to-stand motion
444 driven by bézier curves. *Journal of biomechanical engineering* 140
- 445 Ong, C. F., Geijtenbeek, T., Hicks, J. L., and Delp, S. L. (2019). Predicting gait adaptations due to ankle
446 plantarflexor muscle weakness and contracture using physics-based musculoskeletal simulations. *PLOS
447 computational biology* 15, e1006993
- 448 Ozsoy, B. and Yang, J. (2021). Assisted spatial sit-to-stand prediction—part 2: Virtual injured elderly
449 individuals. *Journal of Computing and Information Science in Engineering* 21, 061009
- 450 Pandy, M., Garner, B., and Anderson, F. (1995). Optimal control of non-ballistic muscular movements: a
451 constraint-based performance criterion for rising from a chair. *Journal of Biomechanical Engineering*
452 117, 15
- 453 Sadeghi, M., Andani, M. E., Bahrami, F., and Parnianpour, M. (2013). Trajectory of human movement
454 during sit to stand: a new modeling approach based on movement decomposition and multi-phase cost
455 function. *Experimental brain research* 229, 221–234

- 456 Schenkman, M., Hughes, M. A., Samsa, G., and Studenski, S. (1996). The relative importance of strength
457 and balance in chair rise by functionally impaired older individuals. *Journal of the American Geriatrics
458 Society* 44, 1441–1446
- 459 Yang, J. and Ozsoy, B. (2020). Three dimensional unassisted sit-to-stand prediction for virtual healthy
460 young and elderly individuals. *Multibody System Dynamics* 49, 33–52
- 461 Yang, J. and Ozsoy, B. (2021). Assisted spatial sit-to-stand prediction-part 1: Virtual healthy elderly
462 individuals. *Journal of Computing and Information Science in Engineering* 21, 041002
- 463 Yokota, H., Ohshima, S., and Mizuno, N. (2016). Sit-to-stand motion analysis using multiobjective
464 genetic algorithm based on musculoskeletal model simulation. *IEEJ Journal of Industry Applications* 5,
465 236–244
- 466 Yoshioka, S., Nagano, A., Hay, D. C., and Fukashiro, S. (2012). The minimum required muscle force for a
467 sit-to-stand task. *Journal of biomechanics* 45, 699–705
- 468 Yoshioka, S., Nagano, A., Himeno, R., and Fukashiro, S. (2007). Computation of the kinematics and the
469 minimum peak joint moments of sit-to-stand movements. *Biomedical engineering online* 6, 1–14

Supplementary Material

1 SUPPLEMENTARY FIGURES

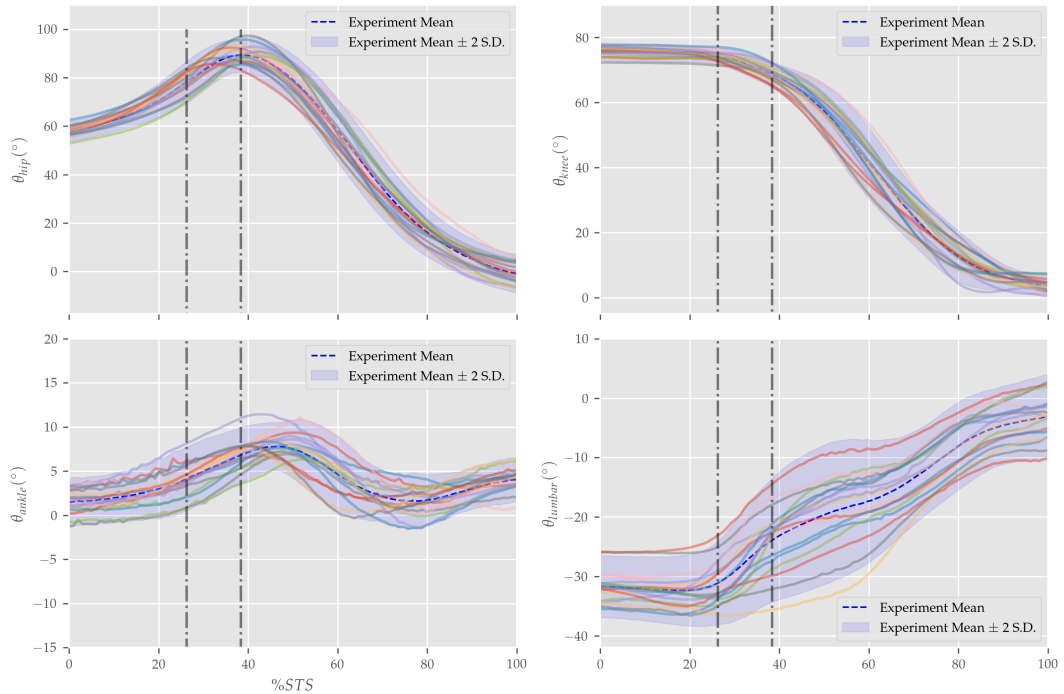


Figure S1. Joint angle trajectories from the experimental trials of the healthy adult. The beginning and the end of STS were defined as the points when hip flexion and hip extensions velocities smoothed with a rolling window of 0.1s grew respectively higher or lower than $20^\circ/s$.

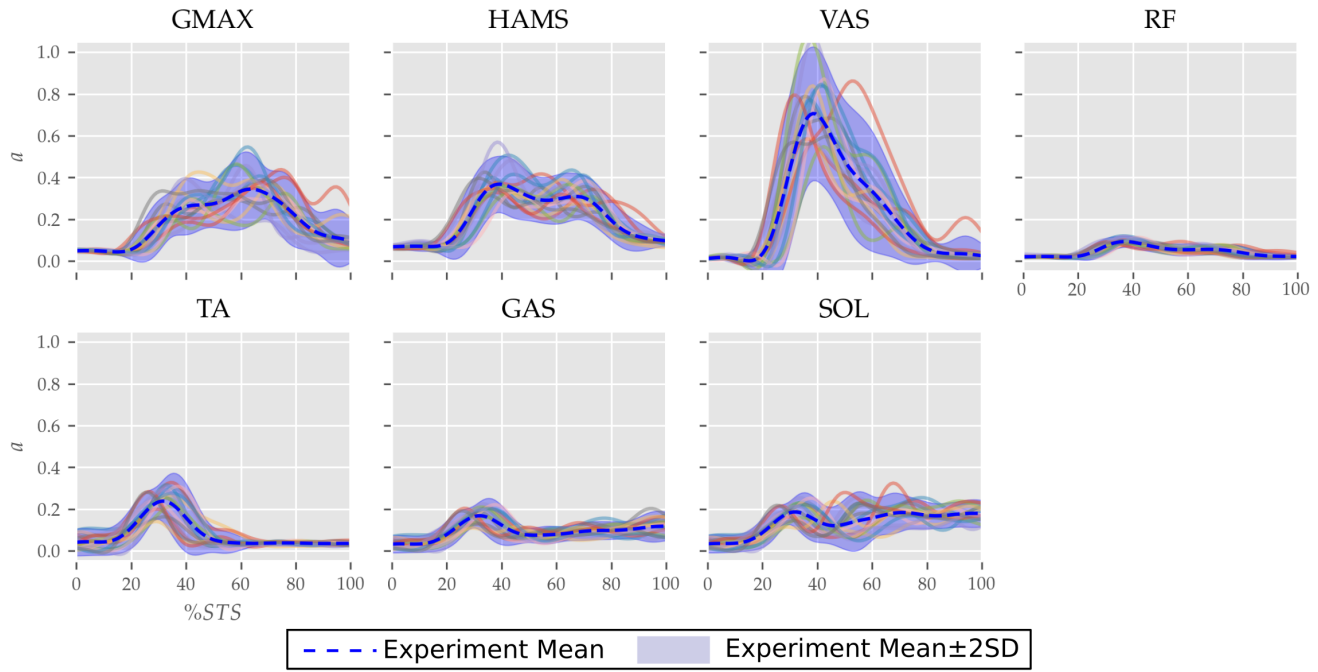


Figure S2. Muscle activation trajectories from the experimental trials of the healthy adult.

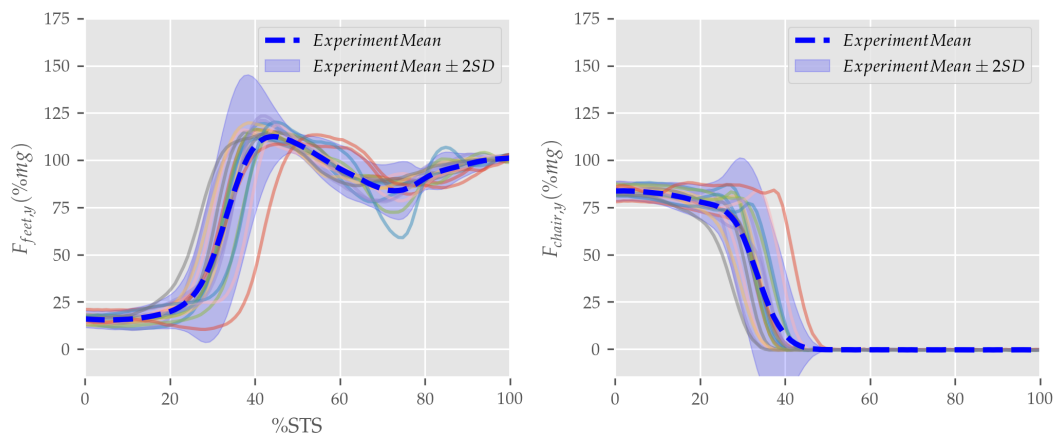


Figure S3. Seat and ground reaction force trajectories from the experimental trials of the healthy adult.

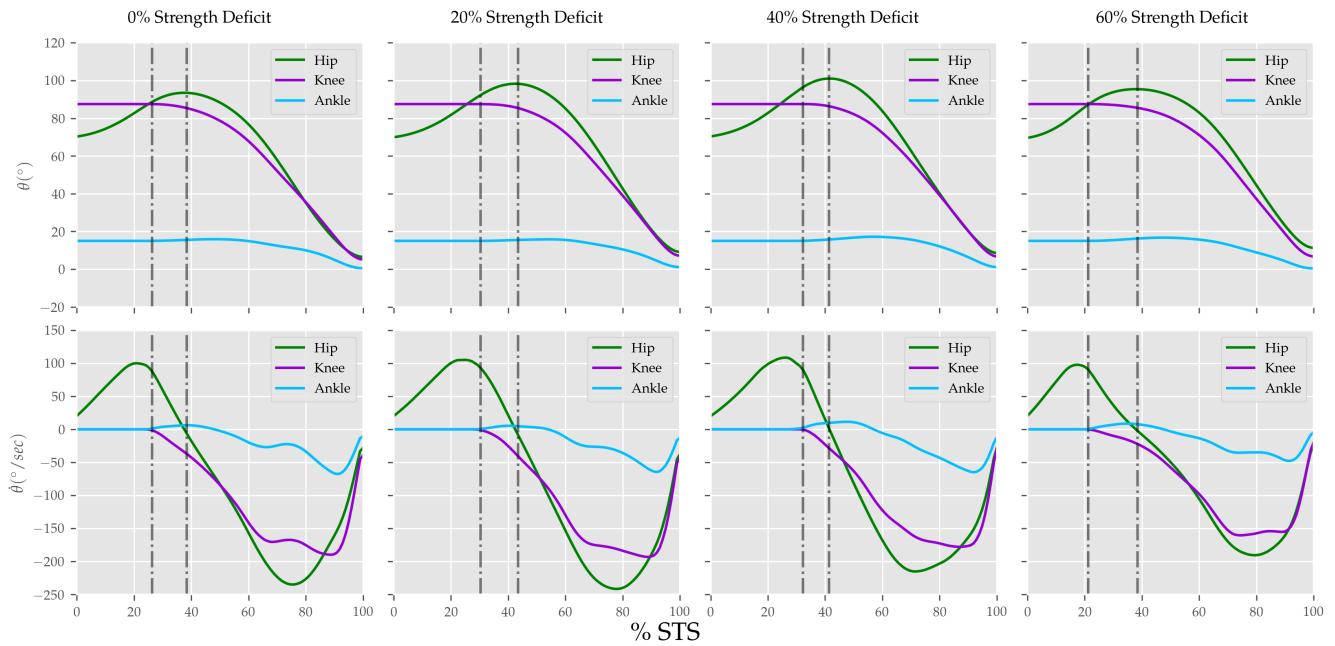


Figure S4. Joint angle and velocity trajectories from the unassisted STS trajectories of model's with different strength deficits.

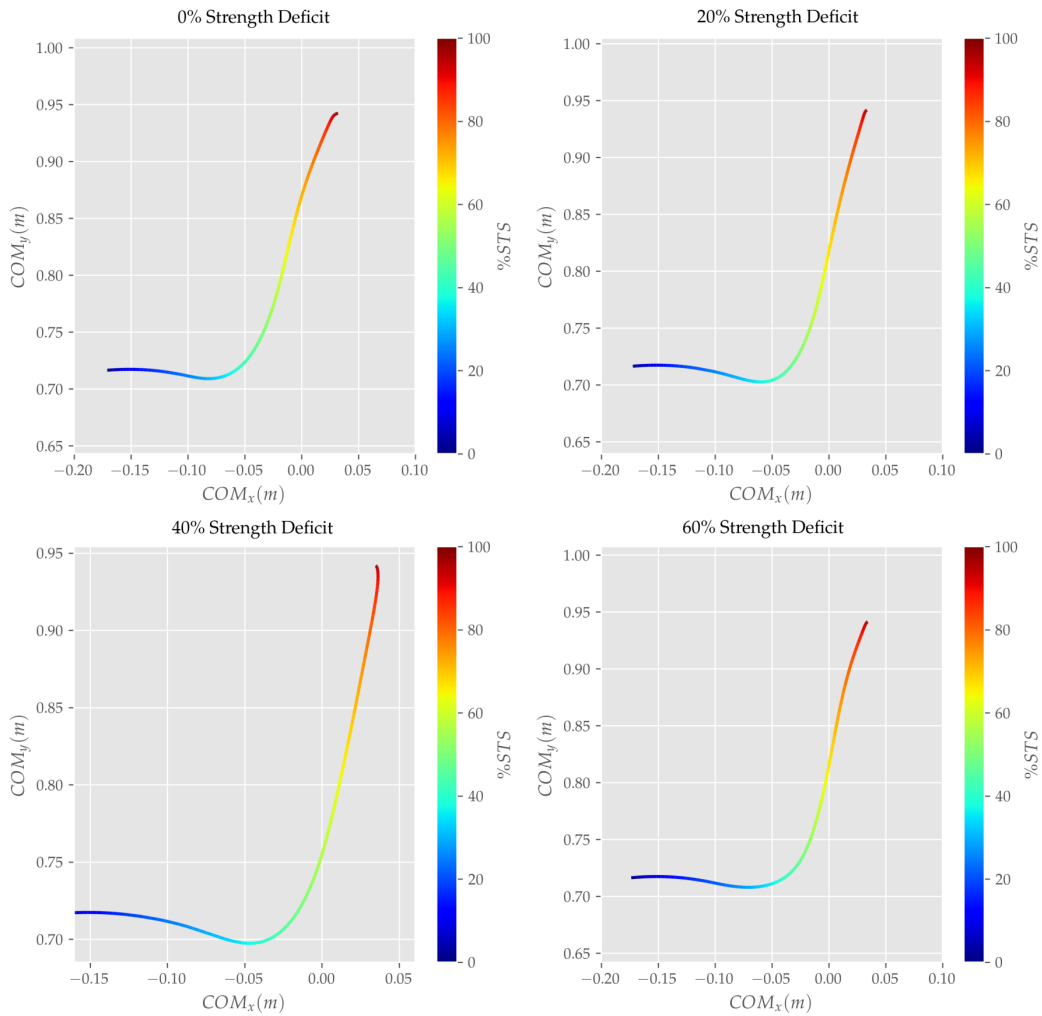


Figure S5. Center of mass trajectories from the unassisted STS trajectories of model's with different strength deficits.

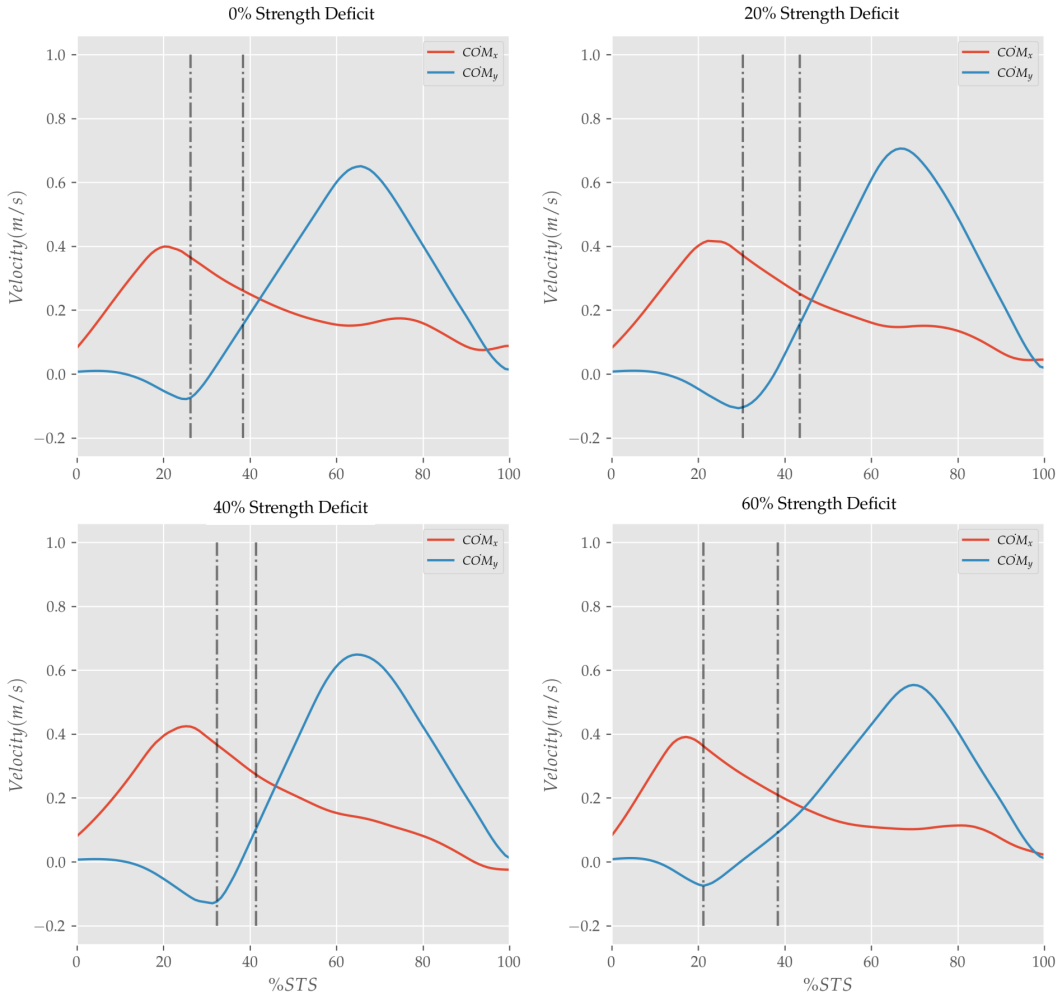


Figure S6. Center of mass velocity trajectories from the unassisted STS trajectories of model's with different strength deficits.

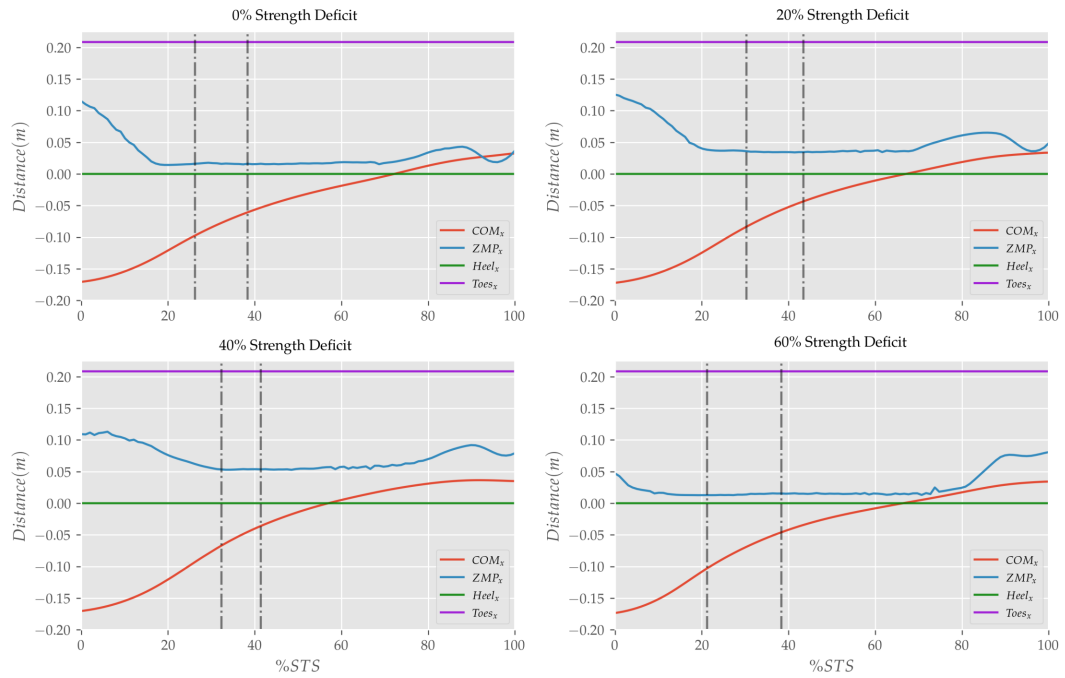


Figure S7. Center of mass and feet force zero moment point trajectories from the unassisted STS trajectories of model's with different strength deficits

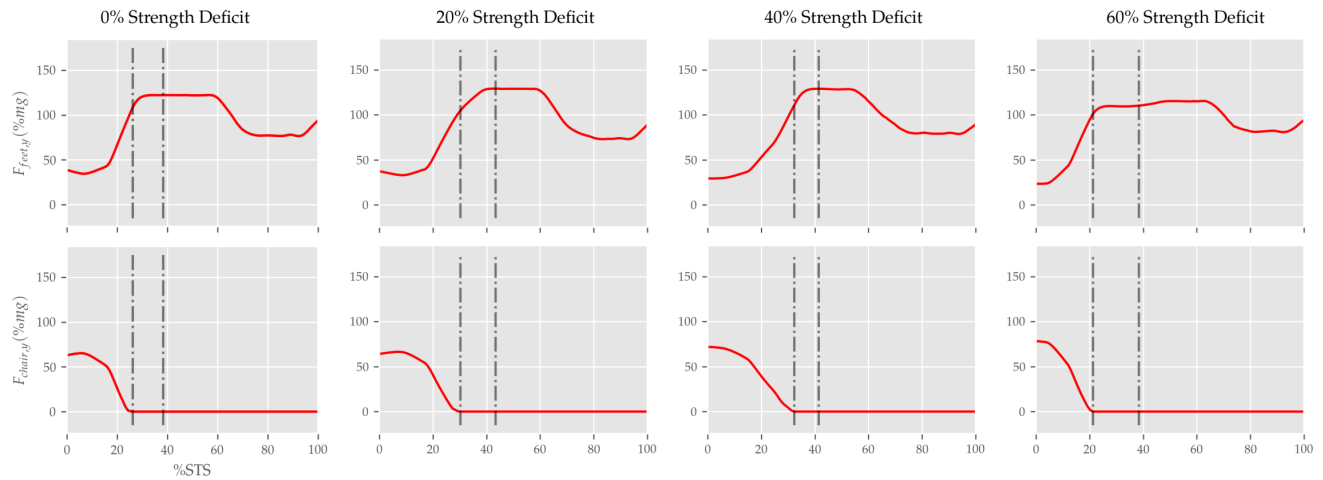


Figure S8. Ground and seat reaction force trajectories from the unassisted STS trajectories of model's with different strength deficits.

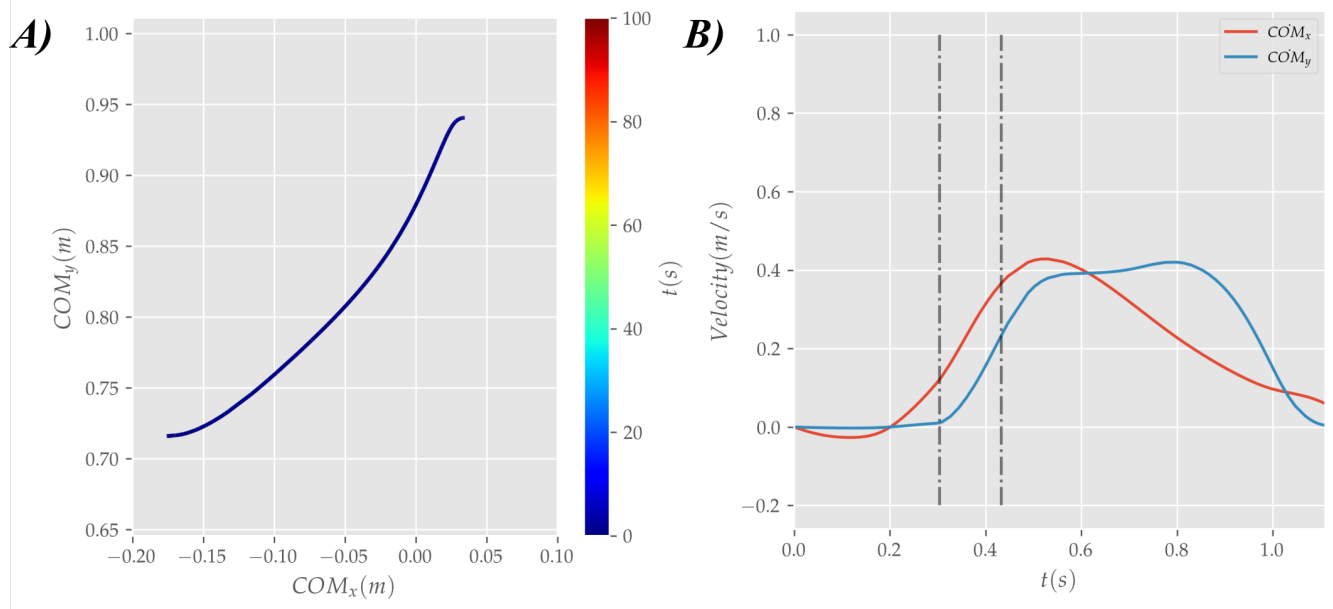


Figure S9. Center of mass trajectories from the Assisted STS trajectories of 80% strength deficit model.

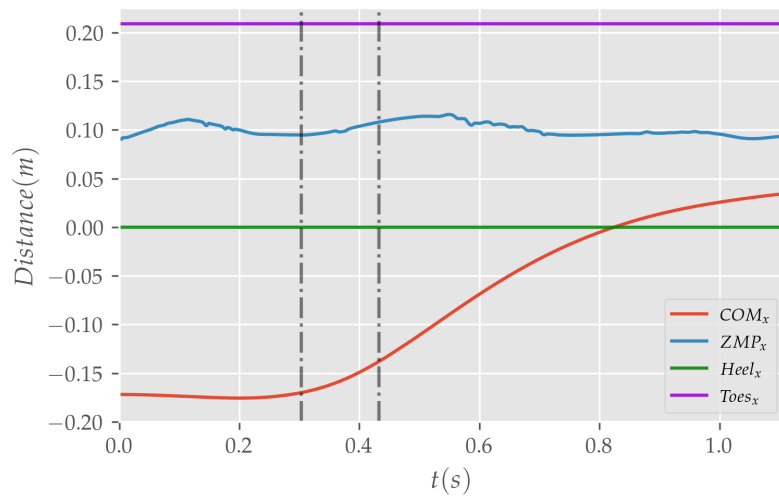


Figure S10. Center of mass and feet force zero moment point trajectories from the Assisted STS trajectories of 80% strength deficit model.